

Runaway stars masquerading as star formation in galactic outskirts

Eric P. Andersson^{*}, Florent Renaud and Oscar Agertz

Department of Astronomy and Theoretical Physics, Lund Observatory, Box 43, SE-221 00 Lund, Sweden

Accepted XXX. Received YYY; in original form ZZZ

ABSTRACT

In the outskirts of nearby spiral galaxies, star formation is observed in extremely low gas surface densities. Star formation in these regions, where the interstellar medium is dominated by diffuse atomic hydrogen, is difficult to explain with classic star formation theories. In this work, we introduce runaway stars as an explanation to this observation. Runaway stars, produced by collisional dynamics in young stellar clusters, can travel kilo-parsecs during their main sequence life time. Using galactic-scale hydrodynamic simulations including a treatment of individual stars, we demonstrate that this mechanism enables the ejection of young massive stars into environments where the gas is not dense enough to trigger star formation. This results in the appearance of star formation in regions where it ought to be impossible. We conclude that runaway stars are a contributing, if not dominant, factor to the observations of star formation in the outskirts of spiral galaxies.

Key words: galaxies: star formation – stars: kinematics and dynamics – ISM: evolution

1 INTRODUCTION

The relationship between star formation rate (SFR) density Σ_{SFR} and gas surface density Σ_{g} , commonly referred to as the star formation (SF) relation, was suggested to follow a power-law by Schmidt (1959). The canonical SF relation is typically quoted with a slope of 1.4 with a break appearing at a critical threshold (see e.g. Kennicutt 1989, 1998; Kennicutt & Evans 2012). The break occurs at $\sim 10 M_{\odot} \text{ pc}^{-2}$ and is attributed to the transition between molecular hydrogen H_2 and neutral atomic hydrogen HI (Wong & Blitz 2002; Kennicutt et al. 2007; Bigiel et al. 2008; Bolatto et al. 2011). However, the underlying reasons of the transition are debated (see e.g. Schaye 2004; Krumholz & McKee 2005; Krumholz et al. 2009; Renaud et al. 2012; Federrath 2013 or Krumholz 2014 for a review).

In the outskirts of spiral galaxies and dwarf irregular galaxies, the SF relation extends into extremely diffuse gas going from $\Sigma_{\text{g}} \sim 10 M_{\odot} \text{ yr}^{-1}$ toward $\Sigma_{\text{g}} \sim 1 M_{\odot} \text{ yr}^{-1}$ (Roychowdhury et al. 2009; Bigiel et al. 2010; Bolatto et al. 2011; Elmegreen & Hunter 2015) in which SF proceeds extremely slowly with a roughly constant depletion time of 100 Gyr. Elmegreen (2015, 2018) found that a SF relation with a slope of 2 for the outer galaxy if the disc flares, i.e. if the thickness is regulated by gas self-gravity and a radially uniform velocity dispersion. Krumholz (2013) suggested another model, in which star formation can occur in an atomic medium with a separate cold and warm phase. Krumholz argued that in regions with low star formation rate (e.g. galactic outskirts), the transition between HI and cold star forming H_2 is mediated by hydrostatic balance. SF then proceeds slowly, with depletion times of ~ 100 Gyr, in agreement with observations (e.g. Bigiel et al. 2010; Bolatto et al. 2011). Here

we show that runaway stars, formed in dense gas and ejected into low density regions, naturally explain the observed third regime of SF in galactic outskirts.

Runaway stars are produced by close encounters and binary disruption due to stellar evolution in young stellar clusters (Blaauw 1961; Poveda et al. 1967). These stars have been studied extensively, both observationally (e.g. Gies & Bolton 1986; Gies 1987; Stone 1991; Hoogerwerf et al. 2000; Silva & Napiwotzki 2011; Maíz Apellániz et al. 2018; Dorigo Jones et al. 2020; Raddi et al. 2020) and through modeling (e.g. Ceverino & Klypin 2009; Eldridge et al. 2011; Moyano Loyola & Hurley 2013; Oh & Kroupa 2016; Kim & Ostriker 2018; Andersson et al. 2020). Typically 5 – 10 per cent of massive OB-type stars have velocities exceeding 30 km s^{-1} and can travel hundreds of pc to several kpc before exploding as core-collapse supernovae (SNe). Moreover, the less massive B stars ($\sim 4 M_{\odot}$) are more numerous and can travel significantly further due to their longer lifetimes (~ 150 Myr). As such, they can reach the galactic outskirts and contribute to the observational tracers of the SF activity, yet without direct physical connection to the formation sites. By expanding on the results of Andersson et al. (2020), we show in this Letter that this mechanism yields an observable signature in striking agreement with SF in galactic outskirts, where gas surface densities are extremely low, as observed by Bigiel et al. (2010).

2 NUMERICAL SETUP

This work uses the two isolated Milky Way-like galaxies described in Andersson et al. (2020). We compare one (referred to as *runaways*), which includes runaway stars where individual stars

^{*} E-mail: eric@astro.lu.se

are tracked both in terms of stellar evolution and kinematically, to an identical simulation ignoring runaway stars (referred to as *no runaways*). We briefly describe the numerical method here, and refer to [Andersson et al. \(2020\)](#) for details.

We ran the two simulations for 250 Myr using the N -body + Adaptive Mesh Refinement (AMR) code RAMSES ([Teyssier 2002](#)), which treats dark matter and stars as collisionless particles and computes the fluid dynamics on a grid with adaptive resolution assuming ideal mono-atomic gas with adiabatic index $\gamma = 5/3$. Gas cooling is metallicity-dependent and treated using tabulated values. SF is controlled by a density threshold (100 cm^{-3}) with the SFR density computed from the cell gas density divided by the local free-fall time and scaled with an efficiency of 5 per cent. The details of this method are discussed in [Agertz et al. \(2013\)](#). The resolution of the grid follows a quasi-Lagrangian refinement strategy for which a cell is refined if it contains more than 8 particles, or more than $4014 M_{\odot}$ of baryonic matter, down to a spatial resolution of 9 pc. The initial conditions are the same as those used for the isolated disc in the AGORA project ([Kim et al. 2014, 2016](#)) and gives a galaxy similar to the Milky Way, but with a gas fraction of 20 per cent.

Star particles are initially sampled with a mass resolution of $500 M_{\odot}$ and immediately split into two groups using the initial mass function (IMF) from [Kroupa \(2001\)](#): i) low mass stars (LMS; $< 8 M_{\odot}$) are grouped and represented by a star particle for which we consider mass loss, Fe and O enrichment as well as momentum and energy injection from type Ia supernovae (SNe) and asymptotic giant branch winds (see [Agertz et al. 2013](#), for details); ii) high mass stars (HMS; $\geq 8 M_{\odot}$) are treated as individual stars with a feedback model accounting for fast winds and core-collapse SNe. The mass-loss rate from the fast winds is computed with a modified version of the model by [Dale & Bonnell \(2008\)](#) and depends on stellar mass and metallicity. Core-collapse SNe occurs when HMS leave the main sequence and results in the injection of 10^{51} erg of energy in the gas. The main sequence time is computed with the age-mass-metallicity fit by [Raiteri et al. \(1996\)](#). In cases when the Sedov-Taylor phase of the SN is unresolved (resulting in problems with a self-consistent development of the momentum build up during this phase), we explicitly inject the associated momentum using the method from [Kim & Ostriker \(2015\)](#). This ensures that we capture the effect of SNe even in region with lower resolution.

In the *runaways* simulation, we add natal velocity kicks to the HMS sampled from the power-law distribution derived from N -body simulations of clusters by [Oh & Kroupa \(2016\)](#):

$$f_v \propto v^{-1.8}, \quad v \in [3, 385] \text{ km s}^{-1}. \quad (1)$$

This results in ~ 14 per cent of stars being runaway¹ with a mean velocity of 90 km s^{-1} .

2.1 Low mass runaway stars

The model in [Andersson et al. \(2020\)](#) limits the runaway mechanism to massive ($> 8 M_{\odot}$) stars because these stars are responsible for the majority of stellar feedback. In this work, where we focus on tracing the resolved SF relation discussed in Section 1, we extend the model to sample individual stars in the mass range $4 - 100 M_{\odot}$ in order to account for the non-negligible contribution to far ultraviolet (FUV)

emission of low mass B-stars. These stars are an important contributor to our SF tracer (see Section 3.2). This extension is achieved by re-sampling the mass² of every HMS in the aforementioned mass range using the Kroupa IMF as a post processing step. For technical reasons, we focus our analysis on ~ 150 Myr of evolution of the galaxy, which roughly corresponds to the main sequence life time of a $4 M_{\odot}$ star. We therefore use this mass as a lower limit, resulting in a mass range between $4 - 100 M_{\odot}$ for the HMS. We keep Equation 1 (which does not have any mass dependence) as the velocity distribution. The re-sampling increases the stellar mass in the HMS population by $1.4 \times 10^7 M_{\odot}$. We remove mass from LMS corresponding to stars in the mass range $4 - 8 M_{\odot}$ since stars in this mass range are now included as HMS, resulting in a decrease in total mass of $1.7 \times 10^7 M_{\odot}$. The discrepancy between the two comes from mass loss due to stellar evolution which is unaccounted for by this re-sampling.

3 RESULTS

3.1 The resolution dependence of the star-formation relation

At the end of the simulation, we derive the local SFR surface density by considering the mass of all stars with an age less than Δt in square bins with sides Δx placed in a uniform grid on the face-on view of the galaxies. We compare this to the gas surface density in the same bins and show the result in Figure 1 for different choices of Δt (0.1 kpc and 1 kpc) and Δx (2 Myr and 10 Myr). We find that both galaxies follow the empirical relation $\Sigma_{\text{SFR}} \propto \Sigma_{\text{g}}^{1.4}$ ([Kennicutt 1998](#), red dashed line in Figure 1) at high gas densities, with a break at $\sim 10 - 100 M_{\odot} \text{ pc}^{-2}$ going into the regime of slow SF³. Our galaxies show slightly faster SF at high surface densities ($\Sigma_{\text{g}} \gtrsim 100 M_{\odot} \text{ pc}^{-2}$), albeit being within the typical observed scatter in local spiral galaxies (see e.g. [Wong & Blitz 2002](#); [Crosthwaite & Turner 2007](#); [Kennicutt et al. 2007](#); [Schuster et al. 2007](#); [Bigiel et al. 2008](#)). We find that increasing the resolution in time and space, i.e., decreasing Δt and Δx , results in less dispersion in the SF relation for both *runaways* and *no runaways*. We attribute this to a tighter correlation between newly formed stars and their natal gas clouds. Increasing Δt causes the scatter to increase because of the decoupling between stars and gas due to e.g. stellar feedback, dynamical drift, cloud dissolution. These different decoupling mechanisms have a range of spatial scales and time scales. By increasing Δx , the variations of the gas density from region to region are averaged out, thus reducing the scatter in Figure 1. However, increasing the temporal and spatial scales inevitable causes the measurements to deviate from the relation imposed from the *local* (cell-based) SF law. Similarly to our results, [Khoperskov & Vasiliev \(2017\)](#) found that on small spatial scales ($\lesssim 100 \text{ pc}$) the SF relation as measured from far ultraviolet (FUV) flux deviates from that estimated by free-fall collapse of molecular clouds (see

² Assigning new masses inevitably leads to a different stellar evolution. This implies a discrepancy between the stellar evolution of the analysed stars and those evolved in the simulation. This is a limitation of our model, which we take into consideration when drawing conclusions from our results.

³ We use the terms slow/fast SF to describe trends following long/short depletion times (i.e. lines of constant $\tau_{\text{dep}} = \Sigma_{\text{g}}/\Sigma_{\text{SFR}}$). This is sometimes referred to as SF efficiency (then defined as the inverse of depletion time). In this work, we reserve the term efficiency to describe the conversion of gas mass into stellar mass (without concern for the timescale). For a more detailed discussion on differences between SF efficiency and depletion time, see e.g. [Semenov et al. \(2018\)](#); [Renaud et al. \(2019\)](#)

¹ We define runaway stars as stars with peculiar velocities $> 30 \text{ km s}^{-1}$. For a discussion on this value, see [Andersson et al. \(2020\)](#) and references therein.

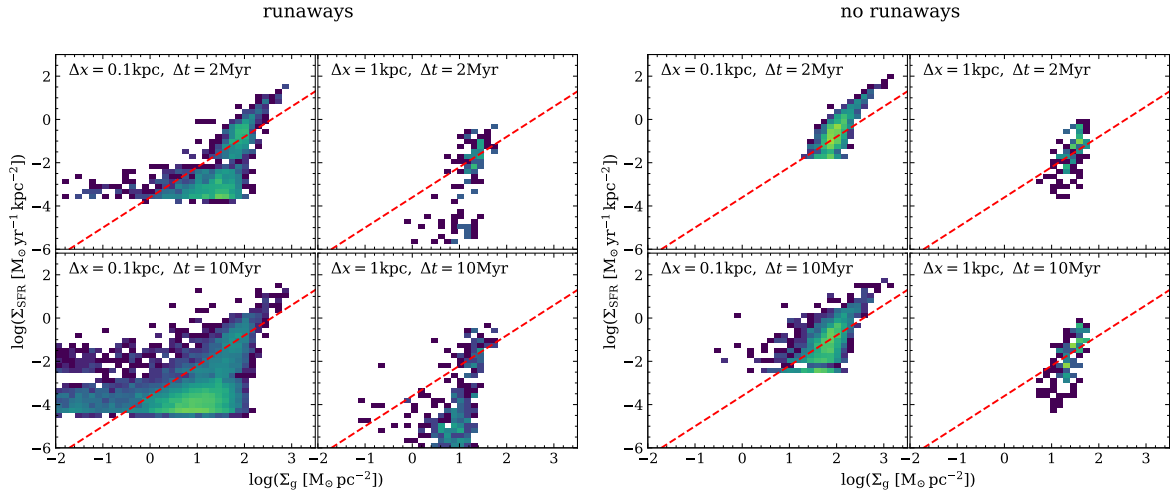


Figure 1. SFR surface density as function of gas surface density for different resolution in space (Δx) and time (Δt) for the model with runaway stars (left) and without (right). Small values for Δx and Δt results in the tightest coupling between stars and gas. To guide the eye, the canonical SF relation with a slope of 1.4 (Kennicutt 1989, 1998) is shown by the red dashed line.

e.g. equation 21 in Krumholz & McKee 2005). This implies that on such scales the SF relation reflects the various evolutionary stages of individual star forming clouds, hence the relation is lost as clouds are destroyed or stars escape (see also Onodera et al. 2010).

Naturally, we find more scatter in the SF relation in the runaways model, since the velocity kicks amplify the decoupling of the runaway stars from their natal gas. This masquerades as star formation activity in regions of low Σ_g , as best seen in left panels at $-1 \lesssim \log(\Sigma_g) \lesssim 0$ and $\log(\Sigma_{\text{SFR}}) \sim -2$.

In all panels of Figure 1, there is a floor in Σ_{SFR} (most clearly visible for $\Delta x = 0.1$ kpc). This floor is a result of having a single star particle within a bin of size Δx , and is therefore set by the finite resolution in stellar masses. In runaways the resolution is $4 M_\odot$, while in the no runaways, it is the mass of the entire unresolved stellar population. As discussed earlier, increasing Δt allows stars to travel further, reaching a larger range of densities. For very long time scales (~ 100 Myr), runaway stars reach the outskirts of the galaxy, as discussed in the remainder of Section 3.

3.2 Runaway stars explain observations of low SFR

To avoid arbitrary time scales (Δt), we create mock observations of the FUV flux. These are shown in Figure 2 as surface brightness maps (left panel) from which we derive the SFR density. In the right panels, we plot them against the surface density of neutral and molecular hydrogen $\Sigma_{\text{HI+H}_2}$ (centre panels). This accounts for the dimming of FUV luminosity due to stellar evolution, thus introduces a self-consistent timescale, and lifts the requirement for an arbitrary Δt . This measurement of SFR is therefore consistent with that estimated observationally. Appendix A details how we produce and observe the mock spectra. The SFR is then computed as

$$\text{SFR} [M_\odot \text{ yr}^{-1}] = 0.68 \times 10^{-28} I_{\text{FUV}} [\text{erg s}^{-1} \text{ Hz}^{-1}], \quad (2)$$

where I_{FUV} is the FUV intensity integrated over the GALEX-FUV filter. We calibrate the I_{FUV} such that the global SFR is the same as that measured in the simulation, as detailed in Appendix A. Equation 2 is identical to that derived by Salim et al. (2007) and later adopted by Leroy et al. (2008) and Bigiel et al. (2010). Note that this is the unobstructed SFR (not accounting for the contribution

of embedded SF observed in infrared re-emission), and is therefore a lower limit of the SFR. However, our main finding is the feature in the low gas density regime, where the SFR densities are largely unaffected by extinction.

As shown in the top right panel of Figure 2, we find a radial dependence in the branch at low Σ_g and low Σ_{SFR} . In fact, we find that the transition into this feature corresponds to the regions outside of the star forming disc ($\gtrsim 10$ kpc), thus explaining the absence of this branch in the no runaways simulation. The signal arises because the runaway mechanism ejects stars into regions where the density is too low for SF to be active. This creates the illusion of SF in gas with extremely low density, seen as the aforementioned feature extending from $\Sigma_{\text{SFR}} \sim 10^{-4} M_\odot \text{ yr}^{-1} \text{ kpc}^{-2}$, toward the bottom left. Initially, the branch roughly extends along a line of constant depletion time (shown by dashed the lines) corresponding to extremely slow star formation ($\tau_{\text{dep}} = 100$ Gyr), and flattens out as it reaches very low $\Sigma_{\text{HI+H}_2} (\leq 0.1 M_\odot \text{ pc}^{-2})$. A comparison to measurements of SF in outer regions of observed spiral galaxies (Bigiel et al. 2010) reveals a striking similarity to the feature produced by our runaway model. How far out the branch extends radially depends on the runaway model, i.e. the velocity distribution and the mass distribution of the stars, as discussed in Section 4.

The middle panels of Figure 2 compare the gas structure between runaways and no runaways. The runaways (top) simulation features large under-dense regions within the star forming disc (a few kpc from the centre). The repeated transport of runaway stars into low density medium (e.g. inter-arm) allows these feedback bubbles to expand to large volumes and survive for longer timescales compared to the no runaways case where they are confined to dense media. As in the galactic outskirts ($\log(\Sigma_{\text{SFR}}) \sim -6$), these low gas surface density regions at $\log(\Sigma_{\text{SFR}}) \sim -2$ harbour an unexpected SF activity introduced by the presence of runaway stars. Contrary to the galactic outskirts, these measurements are indicative of fast SF ($\tau_{\text{dep}} \sim 10$ Myr) as seen in the top right of Figure 2, because runaway stars are more abundant in the inner parts of galactic disc.

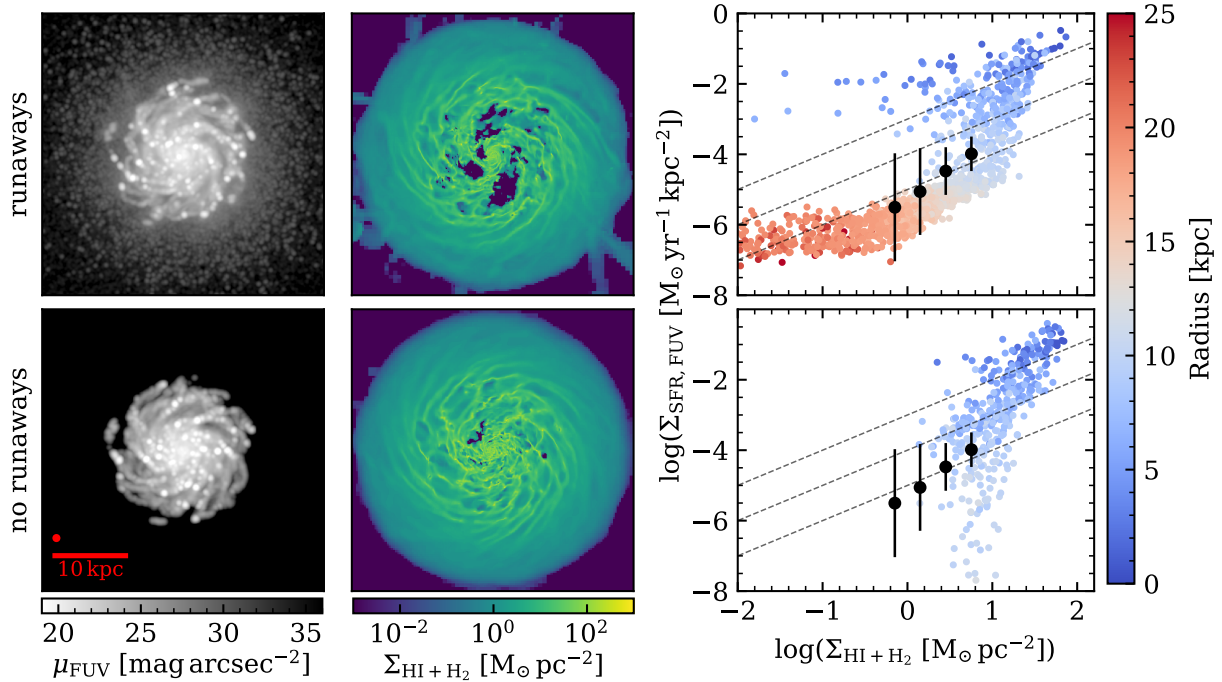


Figure 2. *Left:* FUV surface brightness maps derived by assigning spectra to each star (see text for details). Each pixel has been convolved with a Gaussian filter with FWHM of $4''$ converted to physical units by assuming a distance of 20 Mpc to the galaxies. The point spread function is shown by the red circle. *Center:* Surface density of HI and H₂ gas along the line of sight. The scale is the same as for that in the left panel. *Right:* Resolved SFR density as function of gas surface density colour-coded by distance to the centre of the galaxy. $\Sigma_{\text{SFR, FUV}}$ is computed from FUV intensity (Equation 2), in 1 kpc squares. The colour-coding clearly shows that the low- Σ_{SFR} feature is a radial trend related to the inclusion of runaway stars. The black dots with errorbars shows the mean and scatter for the resolved KS-relation observed in outer regions of spiral galaxies by Bigiel et al. (2010). The dashed lines corresponds to constant depletion times of 100 Gyr, 10 Gyr and 1 Gyr from bottom to top respectively.

4 DISCUSSION

The physical process responsible for the observational detection of young stars at gas surface densities as low as $1 M_{\odot} \text{pc}^{-2}$ in resolved galaxies (e.g. Bigiel et al. 2008; Wyder et al. 2009; Elmegreen & Hunter 2015; Bigiel et al. 2010) has been debated (Krumholz 2014, for a review). Elmegreen (2015) argued that the longer depletion times in the outskirts arises from disc flaring reducing the local volume density of gas, while keeping the surface density relatively high. This is in contradiction with our no runaways model, were such a feature should be visible. Krumholz (2013) suggested that the trend at low Σ_{SFR} can be explained by inefficient star formation in molecule-poor gas in the outskirts of galaxies. A key property of their model is the background interstellar radiation, which we do not account for in the star formation law in our simulations. Therefore, we cannot not rule out low levels of star formation in molecule-poor gas in the galactic outskirts. Nevertheless, runaway stars, as modelled in this work, must contribute to the observed SF signal, at least to some extent. Fully understanding the contribution from runaway stars likely requires advanced models with full N -body treatment of all stellar clusters, including consistent descriptions of the clusters natal properties, such as binary fraction. Furthermore, this needs to be accounted for over cosmological times to obtain a self-consistent local FUV background. This is beyond the scope of current models.

Star formation in very diffuse gas could either reflect *in-situ* star formation, or result from rapid migration of stars, as we advocate for here. As discussed above, the former case calls for an additional regime of star formation. However, the two possibilities would lead

to a different stellar mass function. By comparing FUV flux with H α emission from HII regions, Meurer et al. (2009) found a deficit of massive O stars associated with the FUV bright outskirts (see also Werk et al. 2010). Note that there is a debate surrounding their conclusions (see e.g. Fumagalli et al. 2011; Andrews et al. 2013, 2014). Unless arguing for a non universal IMF (e.g. Pflamm-Altenburg & Kroupa 2008), a deficit in O stars supports our scenario since we find that the main contributor to the FUV signal are stars in the mass range $5 - 7 M_{\odot}$, with almost no contribution from O stars with mass $> 20 M_{\odot}$.

In this work, we apply a model which treats stars as individual particles on galactic scales, which is numerically challenging. In order to reduce computational cost, the model in Andersson et al. (2020) is limited to massive stars ($> 8 M_{\odot}$) because these trace the majority of stellar feedback. In this work, we have extended the model to include individual stars down to $4 M_{\odot}$, thus accounting for their contribution to the FUV flux in galaxies⁴. The velocity distribution (Equation 1) is that of all stars in a natal cluster, implying that in principle we can choose to re-sample for any stellar masses. However, because of mass segregation and the dynamics of many-body interactions, the velocity distribution is known to be mass dependent. More massive stars are more likely to receive stronger kicks. Maíz Apellániz et al. (2018) estimated that in the field 10–12 per cent of O stars are runaways, while this is fraction is reduced

⁴ Although the contribution to FUV intensity is limited for low mass stars, their long main sequence lifetime makes them important for the radial dependence of the SF relations.

to ~ 6 per cent for B stars (see also Eldridge et al. 2011). In future work, we will investigate how our results depend on varying the distribution of kick velocities.

5 SUMMARY & CONCLUSIONS

Using hydrodynamic simulations of an isolated Milky Way-like galaxy (Andersson et al. 2020), we show how runaway stars change the appearance of SF, as seen in the Σ_g - Σ_{SFR} plane. We demonstrate how the SF relation depends sensitively on the spatial and temporal scales over which they are averaged. This sensitivity is increased by runaway stars, since their high velocities implies that they quickly leave their natal environments. By estimating the SFR from the FUV intensity, we remove the necessity of choosing an *ad hoc* timescale and produce a SF relation consistent with that derived from observations.

Our main result is a feature in the SF relation at $\Sigma_{\text{SFR}} \sim 10^{-4} - 10^{-6} M_{\odot} \text{ yr}^{-1} \text{ kpc}^{-2}$ in low surface density gas, with a galactocentric radial dependence, found exclusively in our model including runaway stars. This feature is in excellent agreement with that observed in the outer regions of spiral galaxies (Bigiel et al. 2010). We show that this feature arises by ejecting massive FUV emitting stars (via the runaway mechanism) from star formation regions into low-density gas. This results in the presence of young stars in gas with densities that are too low to trigger star formation. Therefore, it produces an unexpected signature of SF, with a strong radial dependence.

In conclusion, we argue that the SF relation in the outer regions of spiral galaxies is produced by a small, albeit observable, population of individual stars formed in denser environments and transported there by the runaway mechanism. Although our model can not rule out star formation in atomic gas (Krumholz 2013), runaway stars is at the very least a contributing, if not dominant, factor to establishing the SF relation in outer regions of galaxies.

ACKNOWLEDGEMENTS

We thank the anonymous referee for comments which improved this work. We also express gratitude for the stimulating discussions at the 2020 Ringberg Virtual Seminar Series. EA acknowledges discussions with Mark Krumholz. We acknowledge support from the Knut and Alice Wallenberg Foundation, the Swedish Research Council (grant 2014-5791) and the Royal Physiographic Society of Lund. We used computational resources at LUNARC hosted at Lund University, on the Swedish National Infrastructure for Computing (SNIC 2018/3-649), as well as allocation LU 2019/2-27.

DATA AVAILABILITY

The data underlying this article will be shared on reasonable request to the corresponding author.

REFERENCES

Agertz O., Kravtsov A. V., Leitner S. N., Gnedin N. Y., 2013, *ApJ*, 770, 25
 Andersson E. P., Agertz O., Renaud F., 2020, *MNRAS*,
 Andrews J. E., et al., 2013, *ApJ*, 767, 51
 Andrews J. E., et al., 2014, *ApJ*, 793, 4

Bigiel F., Leroy A., Walter F., Brinks E., de Blok W. J. G., Madore B., Thornley M. D., 2008, *AJ*, 136, 2846
 Bigiel F., Leroy A., Walter F., Blitz L., Brinks E., de Blok W. J. G., Madore B., 2010, *AJ*, 140, 1194
 Blaauw A., 1961, *Bulletin of the Astronomical Institutes of the Netherlands*, 15, 265
 Bolatto A. D., et al., 2011, *ApJ*, 741, 12
 Ceverino D., Klypin A., 2009, *ApJ*, 695, 292
 Crosthwaite L. P., Turner J. L., 2007, *AJ*, 134, 1827
 Dale J. E., Bonnell I. A., 2008, *MNRAS*, 391, 2
 Dorigo Jones J., Oey M. S., Paggeot K., Castro N., Moe M., 2020, arXiv e-prints, p. arXiv:2009.03571
 Eldridge J. J., Langer N., Tout C. A., 2011, *MNRAS*, 414, 3501
 Elmegreen B. G., 2015, *ApJ*, 814, L30
 Elmegreen B. G., 2018, *ApJ*, 854, 16
 Elmegreen B. G., Hunter D. A., 2015, *ApJ*, 805, 145
 Federrath C., 2013, *MNRAS*, 436, 3167
 Fumagalli M., da Silva R. L., Krumholz M. R., 2011, *ApJ*, 741, L26
 Gies D. R., 1987, *ApJS*, 64, 545
 Gies D. R., Bolton C. T., 1986, *ApJS*, 61, 419
 Hoogerwerf R., de Bruijne J. H. J., de Zeeuw P. T., 2000, *ApJ*, 544, L133
 Jonsson P., 2006, *MNRAS*, 372, 2
 Kennicutt Robert C. J., 1989, *ApJ*, 344, 685
 Kennicutt Robert C. J., 1998, *ApJ*, 498, 541
 Kennicutt R. C., Evans N. J., 2012, *ARA&A*, 50, 531
 Kennicutt Robert C. J., et al., 2007, *ApJ*, 671, 333
 Khoperskov S. A., Vasiliev E. O., 2017, *MNRAS*, 468, 920
 Kim C.-G., Ostriker E. C., 2015, *ApJ*, 802, 99
 Kim C.-G., Ostriker E. C., 2018, *ApJ*, 853, 173
 Kim J.-h., et al., 2014, *ApJS*, 210, 14
 Kim J.-h., et al., 2016, *ApJ*, 833, 202
 Kroupa P., 2001, *MNRAS*, 322, 231
 Krumholz M. R., 2013, *MNRAS*, 436, 2747
 Krumholz M. R., 2014, *Phys. Rep.*, 539, 49
 Krumholz M. R., McKee C. F., 2005, *ApJ*, 630, 250
 Krumholz M. R., McKee C. F., Tumlinson J., 2009, *ApJ*, 699, 850
 Leitherer C., et al., 1999, *ApJS*, 123, 3
 Leitherer C., Ortiz Otálvaro P. A., Bresolin F., Kudritzki R.-P., Lo Faro B., Pauldrach A. W. A., Pettini M., Rix S. A., 2010, *ApJS*, 189, 309
 Leitherer C., Ekström S., Meynet G., Schaerer D., Agienko K. B., Levesque E. M., 2014, *ApJS*, 212, 14
 Leroy A. K., Walter F., Brinks E., Bigiel F., de Blok W. J. G., Madore B., Thornley M. D., 2008, *AJ*, 136, 2782
 Li A., Draine B. T., 2001, *ApJ*, 554, 778
 Maíz Apellániz J., Pantaleoni González M., Barbá R. H., Simón-Díaz S., Negueruela I., Lennon D. J., Sota A., Trigueros Páez E., 2018, *A&A*, 616, A149
 Meurer G. R., et al., 2009, *ApJ*, 695, 765
 Moyano Loyola G. R. I., Hurley J. R., 2013, *MNRAS*, 434, 2509
 Oh S., Kroupa P., 2016, *A&A*, 590, A107
 Onodera S., et al., 2010, *ApJ*, 722, L127
 Pflamm-Altenburg J., Kroupa P., 2008, *Nature*, 455, 641
 Poveda A., Ruiz J., Allen C., 1967, *Boletín de los Observatorios Tonantzintla y Tacubaya*, 4, 86
 Raddi R., Irrgang A., Heber U., Schneider D., Kreuzer S., 2020, arXiv e-prints, p. arXiv:2011.08862
 Raiteri C. M., Villata M., Navarro J. F., 1996, *A&A*, 315, 105
 Renaud F., Kraljic K., Bournaud F., 2012, *ApJ*, 760, L16
 Renaud F., Bournaud F., Agertz O., Kraljic K., Schinnerer E., Bolatto A., Daddi E., Hughes A., 2019, *A&A*, 625, A65
 Roychowdhury S., Chengalur J. N., Begum A., Karachentsev I. D., 2009, *MNRAS*, 397, 1435
 Salim S., et al., 2007, *ApJS*, 173, 267
 Schaye J., 2004, *ApJ*, 609, 667
 Schmidt M., 1959, *ApJ*, 129, 243
 Schuster K. F., Kramer C., Hirschfeld M., Garcia-Burillo S., Mookerjee B., 2007, *A&A*, 461, 143
 Semenov V. A., Kravtsov A. V., Gnedin N. Y., 2018, *ApJ*, 861, 4

- Silva M. D. V., Napiwotzki R., 2011, *MNRAS*, 411, 2596
 Stone R. C., 1991, *AJ*, 102, 333
 Teyssier R., 2002, *A&A*, 385, 337
 Vázquez G. A., Leitherer C., 2005, *ApJ*, 621, 695
 Werk J. K., et al., 2010, *AJ*, 139, 279
 Wong T., Blitz L., 2002, *ApJ*, 569, 157
 Wyder T. K., et al., 2009, *ApJ*, 696, 1834

APPENDIX A: GENERATING SYNTHETIC SPECTRA FOR STELLAR POPULATIONS

The mock observations used in this work are derived by combining a wave propagation method similar to that used in SUNRISE (Jonsson 2006) with stellar spectra from a modified version of the stellar population synthesis code STARBURST99 (Leitherer et al. 1999; Vázquez & Leitherer 2005; Leitherer et al. 2010, 2014). All HMS use evolving spectra for individual stars while the LMS uses an evolving spectra from the stellar population with stars in the relevant mass range. The spectra of each source is propagated through the gas at the highest AMR resolution (~ 9 pc) to the observer. We account for extinction using a dust attenuation curve from Li & Draine (2001) assuming a uniform dust-to-gas ratio of 0.01. We compute the photometric intensity in the GALEX-FUV band for the stars which formed during the simulation (i.e. younger than 250 Myr). To account for missing of FUV flux from unresolved populations and loss of mass due to sampling new masses for HMS particles (see Section 2.1), we artificially boost I_{FUV} such that the global SFR derived from Equation 2 matches that from the simulation. Furthermore we apply a Gaussian filter with FWHM of 4" (i.e. standard deviation of $\sigma = 1.7''$) to all pixels to simulate the angular resolution of GALEX satellite. To convert to physical units we assume a distance of 20 Mpc. The surface brightness maps were computed from the magnitudes using

$$m_{\text{FUV}} = -2.5 \log \left(\frac{f_{\nu}}{\text{erg s}^{-1} \text{ cm}^{-2} \text{ Hz}^{-1}} \right) - 48.6, \quad (\text{A1})$$

where f_{ν} is the spectral flux density in the GALEX-FUV band. When we compute f_{ν} we assume an initial distance of 10 pc and add a distance modulus corresponding to 20 Mpc. For the conversion to surface brightness, we compute the pixel angular size at a distance of 20 Mpc.

This paper has been typeset from a $\text{\TeX}/\text{\LaTeX}$ file prepared by the author.